HAL open science

Polymer electrolyte membrane fuel cell operating in stoichiometric regime

Stéphane Chevalier, Jean-Christophe Olivier, Christophe Josset, Bruno Auvity

To cite this version:

Stéphane Chevalier, Jean-Christophe Olivier, Christophe Josset, Bruno Auvity. Polymer electrolyte membrane fuel cell operating in stoichiometric regime. Journal of Power Sources, 2019, 440, pp.227100. 10.1016/j.jpowsour.2019.227100 . hal-02372709

HAL Id: hal-02372709

https://hal.science/hal-02372709v1

Submitted on 20 Jul 2022

HAL is a multi-disciplinary open access archive for the deposit and dissemination of scientific research documents, whether they are published or not. The documents may come from teaching and research institutions in France or abroad, or from public or private research centers.

L'archive ouverte pluridisciplinaire **HAL**, est destinée au dépôt et à la diffusion de documents scientifiques de niveau recherche, publiés ou non, émanant des établissements d'enseignement et de recherche français ou étrangers, des laboratoires publics ou privés.

Distributed under a Creative Commons Attribution - NonCommercial 4.0 International License

Version of Record: https://www.sciencedirect.com/science/article/pii/S0378775319310936
Manuscript_49141d773f15b92d727c51271a5edea1

Polymer Electrolyte Membrane Fuel Cell Operating in Stoichiometric Regime

S. Chevalier[1,*], J.-C. Olivier[2], C. Josset[3], and B. Auvity[3]

[1]I2M - Institut de Mécanique et d'Ingénierie de Bordeaux (CNRS UMR 5295)
École Nationale Supérieure d'Arts et Métiers (ENSAM)
Esplanade des Arts et Métiers
33405 Talence Cédex, France

[2]IREENA Laboratory (EA 4642)
Université de Nantes
37 boulevard de l'université
BP 406, 44602 Saint-Nazaire Cedex
Saint-Nazaire, France

[3]Laboratoire de Thermique et Énergie de Nantes (CNRS UMR 6607)
Polytech Nantes, Université de Nantes,
La Chantrerie, rue Christian Pauc - CS 50609
44306 Nantes Cedex 3, France.

Abstract

In this work, we report the existence of a stoichiometric regime where the performances of operating polymer electrolyte membrane (PEM) fuel cells are entirely governed by the mass transport in the cathode channels. An analytical model of the fuel cell stoichiometric regime is derived and evidenced experimentally. First from the cell spectral signature at low frequency based on electrochemical impedance spectroscopy, and from the current density distribution measured using a segmented current collector. The existence of such regime provides a simple way to characterize, model and predict PEM fuel cell performances.

Keywords: stoichiometric regime, analytical model, segmented cell, PEM fuel cell, EIS

© 2019 published by Elsevier. This manuscript is made available under the CC BY NC user license
https://creativecommons.org/licenses/by-nc/4.0/

*Corresponding author:
Prof. S. Chevalier
I2M - Institut de Mécanique et d'Ingénierie de Bordeaux (CNRS UMR 5295)
École Nationale Supérieure d'Arts et Métiers (ENSAM)
Esplanade des Arts et Métiers 33405 Talence Cédex, France
Email: stephane.chevalier@u-bordeaux.fr

Nomenclature

Parameters and variables

b	V	Tafel slope
c_c	mol/m^3	oxygen concentration in the channel
c^{ref}	mol/m^3	Reference concentration at the channel inlet
Da	-	Damkholer number
D^{eff}	m^2/s	Effective diffusivity of the GDL
E_{cell}	V	Fuel cell potential
F	C/mol	Faraday constant
h_c	m	Channel depth
h_g	m	GDL thickness
i		Complex unity
i_c	mA/cm^2	Exchange current density
I_{cell}	A/cm^2	Fuel cell current density measured by the FC station
j	A/cm^2	Local current density
j_0	A/cm^2	Inlet current density
l_c	m	Cell width
L_c	m	Channel length
M	g/mol	Molar mass
Pe	-	Peclet number
$\dot{Q}$	ml/min	Air flow rate in operating pressure and temperature
$\dot{Q}_{SCPT}$	ml/min	Air flow rate in standard condition of pressure and temperature
r_{HF}	mΩ	Fuel cell ohmic resistance
R	J/mol/K	Ideal gas constant
R_{ct}	Ω.cm^2	Charge transfer resistance
T	K	Temperature
u_c	m/s	Air velocity
Wa	-	Wagner number
x	-	Molar fraction
y	m	Spatial coordinate
Z	Ω.cm^2	Complex fuel cell impedance

Greek

α_c	-	Dimensionless charge transfer coefficient
δ	-	Periodic state

φ	°	Phase
η	V	Overpotential in the CL
λ	-	Oxygen stoichiometry
ρ	kg/m^3	Density
τ	s	Characteristic time
ω	rad/s	Angular frequency

1. Introduction

Alternative engines to convert and store energy which do not produce any greenhouse gas are a must need. Among the large variety of processes such as wind turbine or solar panel for example, Polymer Electrolyte Membrane (PEM) fuel cells are one of the most promising candidates. They convert hydrogen and air into electricity and heat with water as the only by-product. The efficiency of the direct conversion of the chemical energy into electrical energy is also an important asset of this technology. Today, PEM fuel cells are close to the commercialization, but their cost still needs to be decreased to reach the full market deployment [1,2]. To make the fuel cells less costly, one way is to increase the electrical power density for a given cell. This can be achieved by both improving the electrochemistry [3] and the mass transport in all the fuel cell materials [4].

To study and improve the mass transport in fuel cells, numerous numerical models have been developed by the research community from the cell scale to the pore scale in the GDL or in the catalyst layer [5–7]. Comprehensive reviews of fuel cell mass transport mechanisms are available in the literature [4,8,9] which summarise all the recent advances in fuel cell modeling. An ubiquitous drawback to all the models reported in the previous references is the large number of parameters required (more than ten in general, see ref. [10,11] for example). If few of them can be easily obtained such as the cell dimensions, or operating conditions, most parameters related to the GDL properties (conductivity, permeability), catalyst layer properties (kinetic reaction coefficients) or PEM properties (drag coefficient [12], ionic conductivity) are – in most cases – not accurately known, which introduce a lot of uncertainty in fuel cell model results. In this context, and to overcome this problem, some authors have developed simplified models

which rely onto a very limited sets of fuel cell parameters [13–20]. Such less parametrised models usually work under strong assumptions and over a limited range of operating regimes – which allow for neglecting some of the fuel cell phenomena such as the anode electrochemical reactions for example. In counter part, these simplified models are well suited to make accurate fuel cell properties measurements such as electrochemical properties.

Alongside fuel cell model developments, experimental characterizations of fuel cell properties have been widely reported in the literature. These works were focused at different scales: from the system scale where a whole fuel cell stack is studied [21,22], to component scale where the liquid water transport was imaged in the GDL pores via X-rays radiography for example [23–26]. In between, the single fuel cell behaviour was also studied using mainly electrochemical techniques such as Electrochemical Impedance Spectroscopy (EIS) [27]. This technique is particularly well suited to characterise fuel cell kinetics [28], membrane resistance [29] and mass transport in both GDLs and channels [16,30,31]. A comprehensive review of the fuel cell phenomena which can be characterized through EIS is given in ref. [32]. However, EIS applied to the cell gives a global characterization of the physical phenomena whereas it is well admitted that the fuel cell properties can change along the channel [33,34]. Thus, segmented fuel cells were developed in order to measure local current density [35] and to perform local electrochemical characterizations [33]. Different designs of segmented fuel cell were developed, using segmented straight channels [36] serpentine channels [37], or combining segmented fuel cell with optical visualisations [38]. In all the previous works, the great interest of segmented fuel cells was clearly proven to study the local changes of fuel cell current density, water concentration, or temperature.

In authors' previous works [16], it was shown that a stoichiometric regime can be identified in operating fuel cells. Such regime appears at low to moderate current density (less than 1 A/cm^2) and when the mass transport limitations in the GDL can be neglected [15,16,39] and can be identified using the EIS signature at low frequency (between 3 to 0.5 Hz). It was shown that this low frequency signature is a consequence of the oxygen transport in the channel [40] which is different from the inductive low frequency behavior pointed out by Pivac al. [41,42] to monitor fuel cell aging. Low frequency capacitive loop can also be observed in case of dehydrated membrane as reported by Chevalier et al.[43], but at frequency lower than 1 Hz and in case of very dry operating conditions. Therefore, low frequency capacitive loop measured at low stoichiometry using relatively well hydrated membrane are likely related to oxygen transport in the channel.

Going further, we extend these previous works [16,39] to the local scale, where the current density distribution should depend only on the oxygen stoichiometry in the stoichiometric regime [44]. A segmented fuel cell was specially designed to measure the current density distributions. Once the stoichiometric regime clearly identified, a methodology to characterize the fuel cell electrochemical properties (Tafel slope and exchange current density) is derived from the equations of the fuel cell operating regime. These findings answer the need of less parametrised models for accurate fuel cell properties characterisations and bring two original results compared to the authors' previous works: (i) the evidence of a stoichiometric regime at the local scale (through current density distribution), and (ii) a methodology to accurately characterise the fuel cell kinetics parameters under the stoichiometric regime.

Subsequently in the paper, what is called the global scale is the cell scale at which the cell impedance is measured. The local scale designates the channel scale at which the segmented current density measurements are performed.

2. Methods

2.1 Current density distribution in the stoichiometric regime

The analytical model used to describe the current density and the low frequency impedance in stoichiometric regime is derived from the authors' previous work [15,16]. It was shown that under the assumption of negligible performance losses at the anode and the absence of liquid water in GDLs and channels, fuel cell models can be reduced to a simplified model governed by three dimensionless parameters. The Wagner number, $\mathrm{Wa} = b/(r_\Omega j_0)$, which compares the voltage losses in the CL to the voltage losses in the membrane. The Damkhöler number, $\mathrm{Da} = i_c e^{(E^0-E)/b} h_g/(4Fc^{ref}D^{eff})$, which compares the kinetics of the reaction to diffusive flux of oxygen in the GDL. And the Peclet number, $\mathrm{Pe} = u_c h_c h_g/(D^{eff}L_c)$, which compares the ratio of oxygen transported in the channel to the mass transport in fuel cell porous media. At low current density and low membrane resistance, the stoichiometric regime exists for a particular set of these parameter values, i.e. when the Wagner number is found to be large enough to neglect the overpotential gradients along the channel in the PEM, and when the Damkhöler is small enough to neglect the concentration gradient in the GDL, i.e. the oxygen concentration in the CL is equal to the one in the channel. Under these conditions, the fuel cell is assumed to be operating in the stoichiometric regime [6,15,39], and the fuel cell geometry can be simplified as depicted in Figure 1. Thus, in the stoichiometric regime, the fuel cell can be viewed

as a flow field directly in contact with the catalyst layer; the GDL has no impact onto the fuel cell performances since the concentration gradients in the GDL are neglected as well as its ohmic losses.

The other main assumptions of the model concern the transport of liquid water and the value of the fuel cell parameters. In the present model, the liquid water is not explicitly modelled. It is considered that its impact can be seen through the value of the fuel cell parameters, such as the PEM ohmic resistance or the catalyst layers kinetics among others. In addition, fuel cell parameters are considered to be effective values which are constant along the channel (y-direction in Figure 1(b)). To simplify the calculations and the model, we also consider that the fuel cell is isothermal with ideal current collectors (no ohmic losses in them). The oxygen transport in the channel is assumed to be a plug-flow with an averaged air velocity, u_c. In addition, a plane CL is considered at the cathode, meaning that the electrochemical reaction takes place homogeneously throughout the CL thickness. This last assumption is valid in case of rapid oxygen and charge transport in the CL [14]. Finally, the present stoichiometric model takes into account only the slowest transient phenomena occurring in fuel cells, i.e. the charging/discharging phenomenon in the double capacity layer is neglected.

Thus, under all these assumptions, a relatively simple expression of the transient current density distribution can be written as:

$$j(y,t) = i_c \frac{c_c(y,t)}{c^{ref}} e^{\eta(t)/b}, \tag{1}$$

where j is the current density, i_c is the exchange current density, c_c is the oxygen concentration in the channel, η is the overpotential, and b is the Tafel slope. The transport of the oxygen concentration in the channel is governed as follows:

$$\frac{\partial c_c}{\partial t}(y,t) + u_c \frac{\partial c_c}{\partial y}(y,t) = -\frac{j(y,t)}{4Fh_c}, \tag{2}$$

where u_c is the air velocity, F is the Faraday constant and h_c stands for the channel depth. Equations (1) and (2) are rewritten in dimensionless form using the following parameters: $\tilde{j} = j/j_0$ where $j_0 = j(0)$ is the inlet current density, $\tilde{c}_c = c_c/c^{ref}$, $\tilde{\eta} = \eta/b$, $\tilde{y} = y/L_c$, and $\tilde{t} = t/\tau_c$ where $\tau_c = L_c/u_c$ is the oxygen residence time in the fuel cell. Note that in this model, the oxygen velocity, u_c, is the 2D velocity of the oxygen that would flow in a cell without ribs [16] since these latter are not taking into account in our model. Using these parameters, it leads to:

$$\tilde{j} = \alpha_c \tilde{c}_c, \tag{3}$$

where $\alpha_c = i_c/j_0 e^{\eta(t)/b}$, and

$$\frac{\partial \tilde{c}_c}{\partial \tilde{t}} + \frac{\partial \tilde{c}_c}{\partial \tilde{y}} = -\lambda^* \tilde{j}, \tag{4}$$

where $\lambda^* = j_0 L_c/(4Fc^{ref}u_c h_c)$. Note that a more convenient expression of λ^* is given at the end of this subsection, see Equation (8).

In periodic regime, equations (3) and (4) can be decomposed into steady part (real, denoted with the superscript 0) and a periodic part (complex, denoted with δ) in the frequency domain as:

- $\tilde{j}(\tilde{y},\tilde{t}) = \tilde{j}^0(\tilde{y}) + \delta\tilde{j}(\tilde{y},\tilde{\omega})e^{i\tilde{\omega}\tilde{t}}$, where $\tilde{\omega} = \omega\tau_c$, $\tilde{\omega}$ is the dimensionless frequency, and ω is the angular frequency;
- $\tilde{c}_c(\tilde{y},\tilde{t}) = \tilde{c}_c^0(\tilde{y}) + \delta\tilde{c}_c(\tilde{y},\tilde{\omega})e^{i\tilde{\omega}\tilde{t}}$;
- $\tilde{\eta}(\tilde{t}) = \tilde{\eta}^0 + \delta\tilde{\eta}(\tilde{\omega})e^{i\tilde{\omega}\tilde{t}}$;
- $\alpha_c(t) = \alpha_c^0\left(1 + \delta\tilde{\eta}(\tilde{\omega})e^{i\tilde{\omega}\tilde{t}}\right)$, where $\alpha_c^0 = i_c/j_0 e^{\frac{\eta^0}{b}}$.

Before to be solved in periodic regime, equations (3) and (4) are solved in steady states. Using the inlet conditions $\tilde{c}_c^0(0) = 1$ and $\tilde{j}^0(0) = 1$, it implies that $\alpha_c^0 = 1$ and $\tilde{c}_c^0 = \tilde{j}^0$. So, the steady state equation of the current density distribution writes

$$\tilde{j}^0(\tilde{y}) = e^{-\lambda^* \tilde{y}}. \tag{5}$$

Then, a relationship between λ^* and the oxygen stoichiometric, λ, can be found by computing the mean current density produced by the cell as

$$I_{cell} = j_0 \int_0^1 \tilde{j}^0(\tilde{y}) d\tilde{y} = \frac{j_0}{\lambda^*}\left(1 - e^{-\lambda^*}\right). \tag{6}$$

Rearranging Equation (6) with the definition of λ^* given at equation (4) leads to

$$\frac{I_{cell}\lambda^*}{j_0} = \frac{I_{cell}L_c}{4Fc^{ref}u_c h_c} = \lambda^{-1}, \tag{7}$$

and by combining equation (6) and (7) one can write

$$\lambda^* = -\ln(1 - \lambda^{-1}). \tag{8}$$

Finally, a convenient expression of the current density distribution, $j^0(\tilde{y})$, which depends only on the oxygen stoichiometry is found by combining Equations (2), (4) and (6) as

$$\frac{j^0(\tilde{y})}{I_{cell}} = \lambda^* \lambda e^{-\lambda^* \tilde{y}}. \tag{9}$$

A similar expression for the current density distribution was reported by Kulikovsky [6].

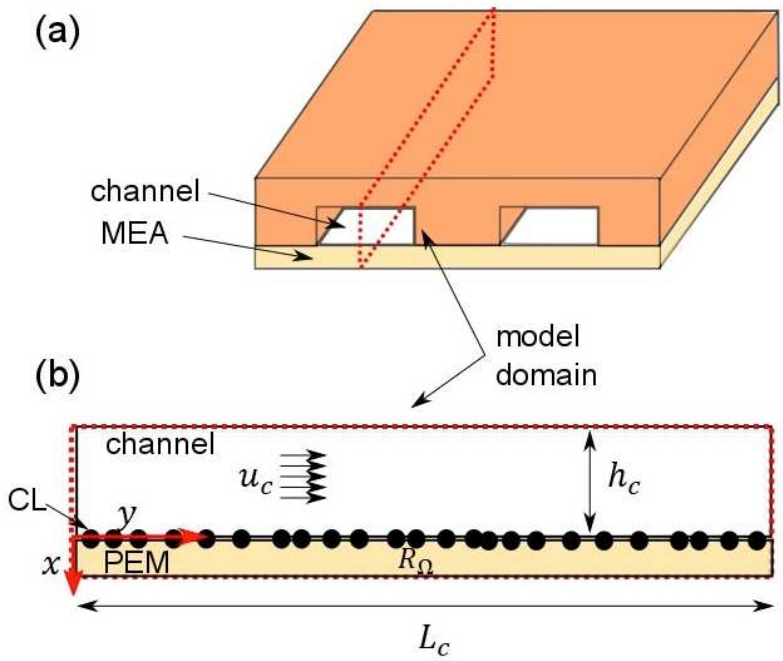

Figure 1. Simplified geometry of a fuel cell operating in stoichiometric regime (GDL neglected). (a), 3D view of a fuel cell with two parallels channels. (b), 2D geometry used to model the fuel cell mass transport phenomena.

2.2 Low frequency spectral signature in stoichiometric regime

Equations (3) and (4) are now solved in the periodic regime. Using the complex decomposition previously introduced, the periodic state of Equation (1) writes

$$\delta\tilde{j} = \delta\tilde{c}_c + e^{-\lambda^*\tilde{y}}\delta\tilde{\eta}. \tag{10}$$

where $\delta\tilde{c}_c$ is obtained from the periodic state of Equation (2) as:

$$i\tilde{\omega}\delta\tilde{c}_c + \frac{d}{d\tilde{y}}\delta\tilde{c}_c = -\lambda^*\delta\tilde{j}, \tag{11}$$

Combining (10) and (11), and solving them, using the inlet condition $\delta\tilde{j}(0) = 0$, leads to the following expression of the periodic current density:

$$\delta\tilde{j}(\tilde{y}) = \frac{i\lambda^*\delta\tilde{\eta}}{\tilde{\omega}}\left(\left(1-\frac{i\tilde{\omega}}{\lambda^*}\right)e^{-\lambda^*\tilde{y}} - e^{-\lambda^*\tilde{y}(1+i\tilde{\omega}/\lambda^*)}\right). \tag{12}$$

Finally, one can compute the dimensionless fuel cell impedance $\tilde{Z}$, whose expression can be obtained from the following equation:

$$\frac{1}{\tilde{Z}} = \int_0^1 \frac{\delta\tilde{j}(\tilde{y})}{\delta\tilde{\eta}}\, d\tilde{y}, \tag{13}$$

developing equation (13) leads to:

$$\frac{1}{\tilde{Z}} = \frac{i}{\tilde{\omega}}\left[\left(1-\frac{i\tilde{\omega}}{\lambda^*}\right)\left(1-e^{-\lambda^*}\right) - \frac{1-e^{-\lambda^*(1+i\tilde{\omega}/\lambda^*))}}{1+i\tilde{\omega}/\lambda^*}\right]. \tag{14}$$

Equation (14) describes the low frequency impedance of the fuel cell in the stoichiometric regime. This equation is identical to the impedance reported in ref. [16] when $\mathrm{Da} \ll 1$ which is the case in such stoichiometric regime. Moreover, like the current density in steady state, it is interesting to note that this dimensionless impedance is governed only by the oxygen stoichiometry.

From Equation (14), two quantities can be computed, namely the phase and the modulus of the impedance. The phase of the impedance Z is then defined as:

$$\tan\varphi = -\frac{\mathrm{Im}(1/\tilde{Z})}{\mathrm{Re}\left(1/\tilde{Z}\right)}, \tag{15}$$

and one can noticed that this quantity is function of τ_c and λ only. Therefore, only the knowledge of the fuel cell operating conditions (air flow rate, pressure, temperature and current) is required to predict the fuel cell phase in stoichiometric regime. This latter will be used in the results section to evidence the stoichiometric regime. In contrast, the modulus is computed as:

$$|Z| = \left| \frac{R_{ct}}{\tilde{Z}(\tau_c, \lambda)} \right|^{-1}, \tag{16}$$

with $R_{ct} = b/j_0$. Thus, the modulus is governed by τ_c, λ, and the cell electrochemical parameters. In absence of knowledge of b and j_0 it is not possible to predict the modulus of the stoichiometric regime. However, Equation (16) is used at the end the next section to validate the model after to have measured the Tafel slope.

2.3 Experimental measurements

Two kinds of experiments are performed in this study to validate both the steady state model using the current density distribution measurements and the periodic state using the EIS response of the fuel cell. To measure the local current density distributions, a segmented flow field was built directly onto a printed circuit board (PCB), see Figure 2, where the current is measured through eleven segments. Each segment is connected in series to a Hall effect current sensor (Allegro Microsystem, ACS723LLCTR-05AB-T), which converts the current that flows through the segment into voltage. All the 11 voltages are then read by a data acquisition system every second. Each sensor was carefully calibrated prior to the fuel cell current measurements (see section S1 in supplementary material). According to the datasheet of the sensor and all the experimental uncertainties, it is assumed that the current densities are measured with an accuracy of ±10%. Such uncertainty was also verified when comparing the current measured by the segmented flow field to the current read by the fuel cell test station (see details in the supplementary materials).

The position, the area and the length of each segment are summarised in Table 1. The segmented flow field was gold plated to ensure minimal contact resistance and to prevent copper

oxidation when place inside the cell. Holes were drilled into the flow field to allow an optical access and verify that no liquid water was present in the channel as assumed in the model. The segmented flow field is inserted at the anode side.

The second kind of measurements are the classical EIS. To do so, the fuel cell was connected to a FCT 50 test station (BioLogic®) to measure the cell current, voltage and impedance. The fuel cell impedance was recorded from 10 kHz to 0.1 Hz with 10 points per decade using an AC sine wave signal equal to 10% of the DC current. The FCT 50 test station was also used to control air and hydrogen flow rates, temperatures, humidity and pressure. The protocol used to record EIS data is detailed in supplementary materials.

In all the experiments, a 12 cm^2 (200 cm-long by 6 mm-wide) single cell was used to validate the model. It comprises two parallel channels of 200 mm-long by 1.5 mm-deep. At the cathode side, the flow field was machined directly in the copper current collector to enable an optical access inside the channels via a transparent plexiglass plate inserted on the top of the channels (see Figure 2(b)). The current collector was gold plated to ensure minimal ohmic resistance (and large Wa). Between the current collectors, a membrane electrode assembly (MEA) was inserted; it is made of a 15 µm-thick Gore PEM with 0.5 mg/cm^2 platinum loading in both anode and cathode CL. The very thin membrane and high platinum loading were specially chosen to ensure low membrane resistance and efficient electrochemical reaction to match our model assumptions (negligible ohmic losses in the membrane and no overpotential gradients in the CL). The MEA was sandwiched between two 10BC GDLs from SGL® compressed at 250 µm using two rigid spacers. Finally, two aluminum end-plates were used to assemble all the fuel cell components. A water cooling circuit connected to a temperature control system was drilled inside the end plates to keep the fuel cell temperature constant at 70°C.

Hydrogen flow rate was kept constant throughout all the measurements at 300 ml/min, 70°C and 30% relative humidly to ensure enough membrane hydration and negligible overpotential losses in the anode. The air flow rate was modulated based on the desired stoichiometry. However, for all the experiments air enters fully dry at a fixed temperature of 70°C at the cell inlet.

The oxygen stoichiometry and oxygen residence time are computed based on the experimental conditions. The mean air density in the cathode channel is estimated as follows:

$$\rho_{air} = \frac{P_{tot}}{RT}\left(x_{H_2O}M_{H_2O} + x_{O_2}M_{O_2} + x_{N_2}M_{N_2}\right), \tag{17}$$

with $x_{O_2} = 0.79/0.21\, x_{N_2}$ and $x_{N_2} + x_{0_2} + x_{H_2O} = 1$. Although the cell is fed using dry air, the water produced by the electrochemical reaction makes the air relative humidity close to 100%. Therefore, it is assumed that $x_{H_2O} = P_{sat}(T)/P_{tot}$. The relationship (15) is then used to compute the air flow rate at the cell temperature and pressure, i.e.: $\dot{Q}(T,p) = \dot{Q}_{SCPT}.\rho_{SCPT}/\rho_{air}$ where $\dot{Q}_{SCPT}$ and ρ_{SCPT} are the flow rate and the density of air in standard condition of pressure and temperature. Then, the oxygen stoichiometry is obtained as

$$\lambda = \frac{\dot{Q}(T,p)c^{ref}}{I_{cell}/(4F)}, \tag{18}$$

where $\dot{Q}(T,p)$ is the volume flow rate given for the cell operating pressure and temperature, I_{cell} is the cell operating current, and c^{ref} is the oxygen concentration at the channel inlet given by the ideal gas law as:

$$c^{ref} = x_{O_2}^{inlet}\frac{p_{tot}}{RT}, \tag{19}$$

where $x_{O_2}^{inlet}$ is the inlet oxygen mole fraction taken to be 0.21 as dry air is used, and p_{tot} is the total air pressure in the fuel cell.

The model derived in the section 2.1 is based on a two-dimensional (2D) geometry which does not take into account the effect of the rib. Therefore, the velocity defined in Equation (1) is a 2D velocity that would flow without any rib. Experimentally the 2D velocity is given by

$$u_c^{2D} = \frac{\dot{Q}(T,p)}{l_c h_c}, \tag{20}$$

where l_c is the cell width, e.g. 6 mm. Finally, the oxygen residence time is based on the u_c^{2D} as

$$\tau_c = \frac{L_c}{u_c^{2D}}. \tag{21}$$

In our flow field geometry, the ratio of the cell active surface to the channel surface is 0.5, thus u_c^{2D} is equal to the half the 3D velocity that flows inside the fuel cell channels.

Segment #	1	2	3	4	5	6	7	8	9	10	11
Length (mm)	19	18	18	18	18	18	18	18	18	18	19
Area (cm^2)	1.14	1.08	1.08	1.08	1.08	1.08	1.08	1.08	1.08	1.08	1.14
Dimensionless position	0.95	0.86	0.77	0.68	0.59	0.50	0.41	0.32	0.23	0.14	0.05

Table 1. Geometrical characteristics of the segmented current collector.

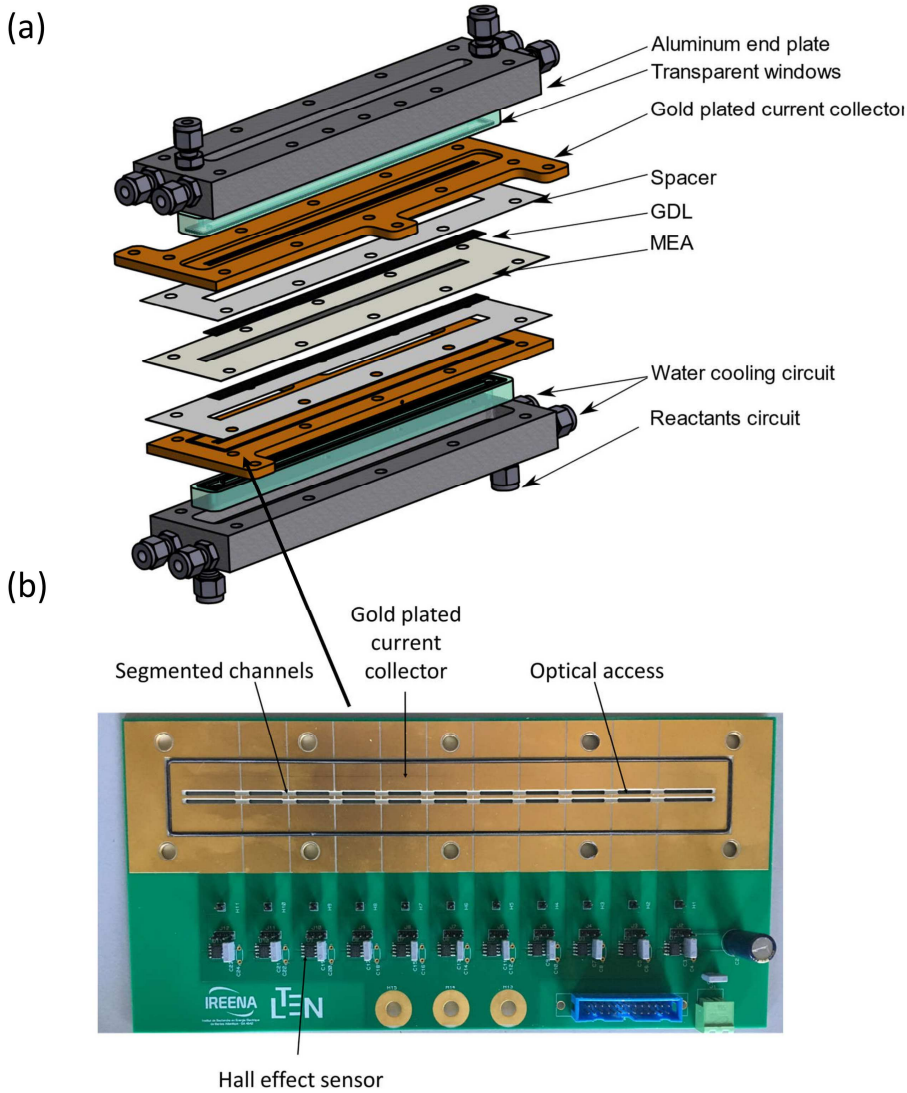

Figure 2. (a) 3D rendering view of the single cell used in the experiments. (b), segmented current collector used to measure the current density distribution. It replaces one of the copper current collector in the single cell.

3. Results & Discussion

3.1 Multiscale evidence of the stoichiometric regime

Before to be able to use the stoichiometric model to characterize the fuel cell electrochemical kinetics, evidences of the stoichiometric regimes have to be observed. This was done at the previously mentioned scales: at the global scale where the EIS signatures at low frequency are measured and at the local scale based on the current density distribution measurements.

3.1.1 At the global scale using low frequency EIS measurements

Like in the authors' previous works [16], the low frequency EIS signature is used to evidence the stoichiometric regime. In the previous section, it was shown that the low frequency phase in the stoichiometric regime is a function of τ_c and λ (see Equation (15)), so it can be predicted easily knowing the fuel cell operating conditions. The low frequency fuel cell phase is measured from the fuel cell impedance as follows:

$$\tan \varphi_{exp} = \frac{\mathrm{Im}(Z_{exp})}{\mathrm{Re}(Z_{exp}) - r_{HF}}, \tag{22}$$

where Z_{exp} is the measured fuel cell impedance, and r_{HF} is the high frequency resistance taken as the average of the real part of the fuel cell impedance between 10 Hz and 5 kHz. r_{HF} is subtracted from the fuel cell impedance to match the assumption of negligible charge transport in the model. The fuel cell phase is measured for a range of oxygen stoichiometries and fuel cell currents. Details about the operating conditions used can be found in Table (2).

The comparison between Equation (15) and the low frequency phase measurements (Equation (22)) for a range of oxygen stoichiometries and a range of currents is presented in Figure 3. The model is computed for the stoichiometry at which the cell is operating (see

Equation (18)) and an interval at ±10% of this oxygen stoichiometry is depicted in dash line. To validate that the cell is operating in stoichiometric regime one can expect that the measured fuel cell phases fall within this interval. As it can be observed in Figure 3 this is particularly true at λ = 1.30 and 1.60 for all the currents (0.25, 0.375 and 0.5 A/cm^2). However, more deviation is noticed at λ = 2.15, and the measured phase is out of the interval at λ = 3.15. Therefore, it can be concluded that the cell is operating in stoichiometric regime for a range of stoichiometric from 1.30 to 2.15 for all the currents tested. This result is in line with the work reported in ref [16], and confirms that the assumption made concerning negligible ohmic losses in the membrane, and the absence of overpotential gradient in the CL are valid.

Another interesting result concerns the scaling of all the measurements regardless the operating current used. This confirms that the low frequency phase depends only on the oxygen stoichiometry when plotted as a function of $\tilde{\omega}$. If the same data were plotted versus the angular frequency, the effect of the operating current would have been shown through a shift of the maximum of the fuel cell phase (see ref [16]).

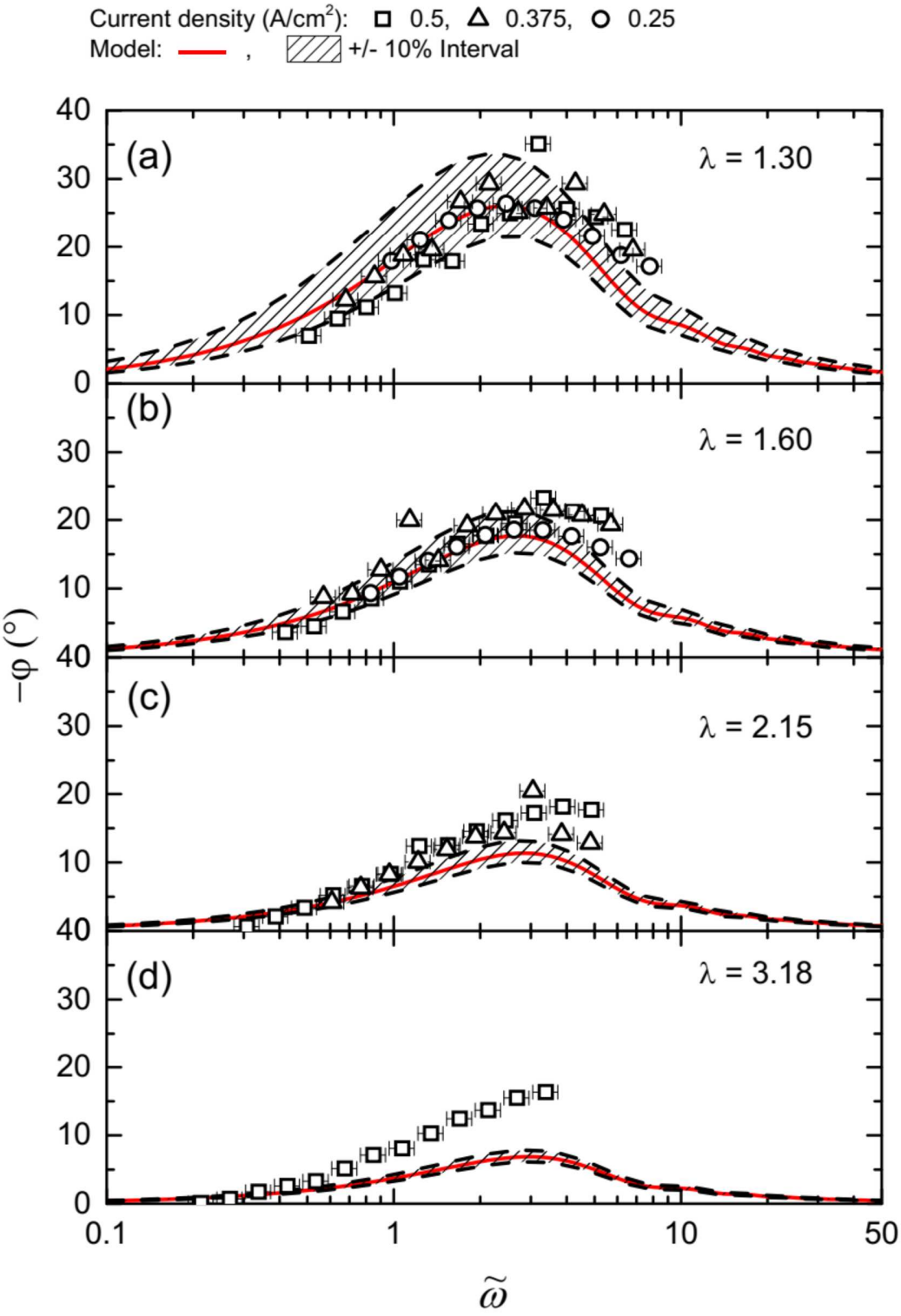
Current density (A/cm²): 0.5, 0.375, 0.25
Model: , +/- 10% Interval
(a)
λ = 1.30
(b)
λ = 1.60
(c)
λ = 2.15
(d)
λ = 3.18
−φ (°)
ω̃
0.1
1
10
50
0
10
20
30
40

Figure 3. Fuel cell low frequency phase measured by EIS for a range of current and oxygen stoichiometry.

Current density (A/cm^2)	**Air flow rate (ml/min)**	**Pressure (bar)**	ρ_{air} **(kg/m^3)**	u_c **(m/s)**	**λ**	τ_c
0.5	123	1.9	2.82	0.31	1.29	0.64
0.25	63	1.87	2.79	0.16	1.32	1.24
0.375	94	1.98	2.904	0.24	1.313	0.86
0.5	153	2.00	2.93	0.39	1.6	0.53
0.25	78	2.02	2.92	0.20	1.63	1.05
0.375	113	1.97	2.894	0.29	1.578	0.72
0.5	204	1.94	2.85	0.52	2.14	0.39
0.25	103	1.90	2.16	0.26	2.16	0.77
0.5	304	2.013	2.93	0.78	3.18	0.27

Table 2. Summary of the operating conditions used in the stoichiometric regime.

3.1.2 At the local scale using current density distribution measurements

The same kind of evidence of the stoichiometric regime is now sought at the local scale. In the stoichiometric regime the current distribution is given by Equation (9). If the measurements of the current in each segment follow the same distribution, then one can conclude that the fuel cell is operating in what we call the stoichiometric regime.

The same operating conditions previously mentioned in Table 2 are used, and the results are presented in Figure 4. The methodology to compute the error bars on the dimensionless currents is detailed in appendix. Globally, it can be noticed that the measurements agree well with the model regardless the operating currents used and the oxygen stoichiometries. For each stoichiometry, all the data points scale with the model with a very small dispersion with respect to the current level, concluding – once again – that only the stoichiometry governed the current distribution not the value of the current itself justifying the name of stoichiometric regime.

Therefore, from the results presented in Figure 4 and associated to those in Figure 3, it is concluded that the fuel cell operates in stoichiometric regime for all the operating conditions given in Table 2.

As noticed in Figure 4(d), surprisingly, the stoichiometric regime may still occur at λ = 3.15 also whereas it was not identified on the low frequency phase (see Figure 3). This result may be due to some transients' phenomena which hinder the frequential signature such as oxygen transport delay in the GDL. When λ is increased, τ_c also increased to the same order of magnitude of the characteristic time of the GDL oxygen transport (see ref [16]). Thus, it may be concluded that the measurements of the current density distribution would be a more reliable technique to evidence the stoichiometric regime since they are not perturbed by GDL transient phenomena.

The model and the measurements are observed to deviate the most at the cell extremities, i.e. at $\tilde{y} \approx 0.05$ and 0.95. At the channel inlet, air enters dry and become humidified after few millimetres. The membrane humidity could therefore be lower at the first segment leading to a lower current production. This effect was observed in the literature on a larger scale [40,45], but here due to the very thin membrane used (15 µm), this non-uniform membrane humidity is only located at the first segment. A second source of uncertainty in the local current density measurement can stem from the uncertainty of the area of the MEA in the segments located at the extremities. During the fuel cell assembly with the segmented current collector, the MEA may have moved a bit toward one of the cell extremities (few millimeters) changing the surface area in contact with the segments at the extremities. This effect was pointed out by Kulkarni et al. [46] using X-rays radiography.

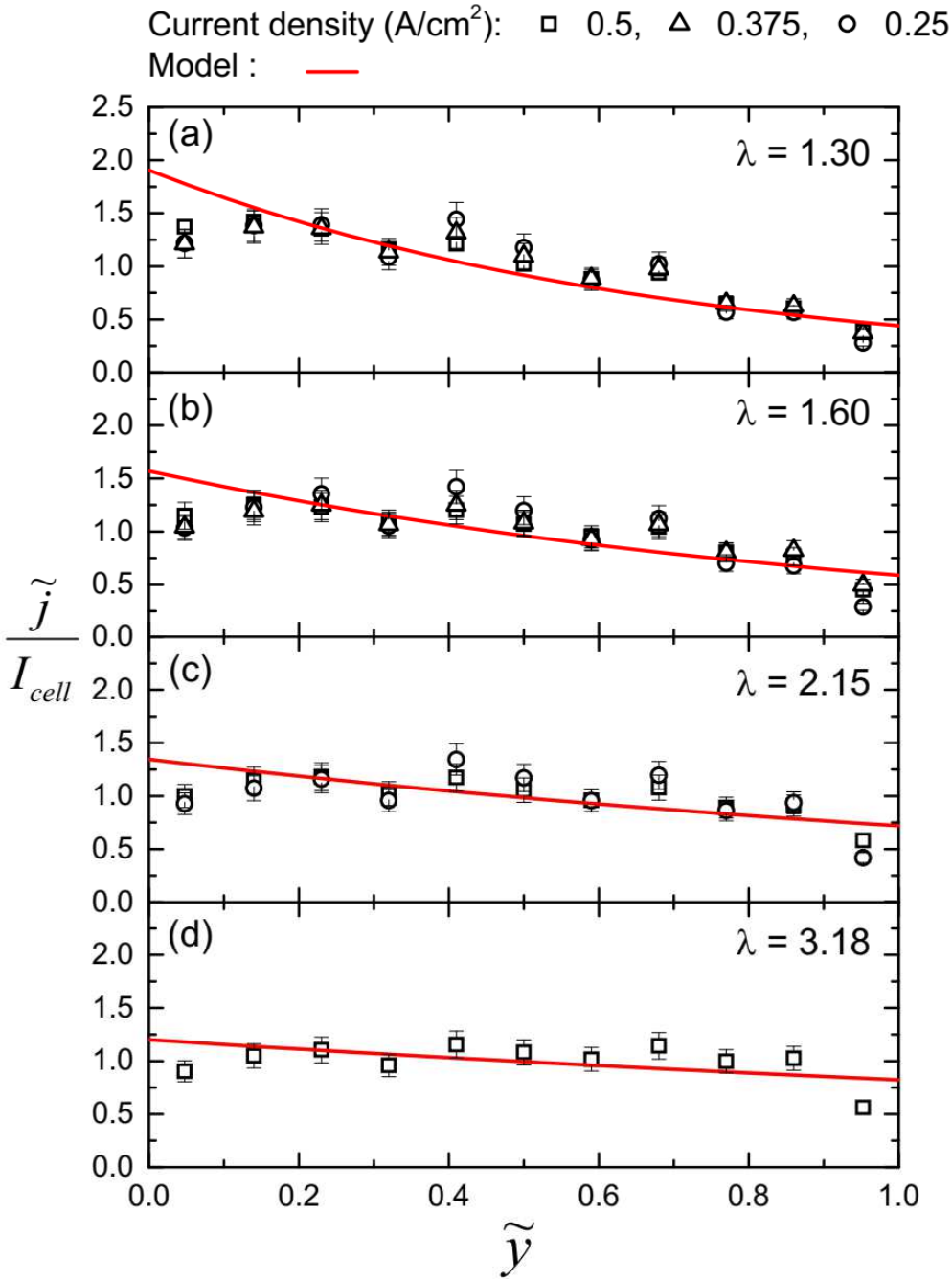

Figure 4. Non-dimensional local current density distributions for a range of current and oxygen stoichiometry.

3.2 Characterisation of kinetic parameters in stoichiometric regime

3.2.1 Parameters identification

In the previous section, it was shown that the fuel cell is operating in the stoichiometric regime, validating the use of Equations (1) and (2) to model the fuel cell behavior. Using these equations, one can show that $c_c^0(y)/c^{ref} = e^{-\lambda^* \tilde{y}}$, and $j_0 = i_c e^{\eta/b}$. Thus, by integrating equation (1) it leads to:

$$I_{cell} = \int_0^1 j(\tilde{y}) d\tilde{y} = i_c e^{\eta/b} \int_0^1 e^{-\lambda^* \tilde{y}} d\tilde{y} = \frac{i_c e^{\eta/b}}{\lambda \lambda^*}. \tag{23}$$

Equation (23), is then rewritten in linear form using the decimal logarithm to obtain:

$$\eta = 2.3b \times \log(I_{cell} \lambda \lambda^*) - 2.3b \times \log(i_c). \tag{24}$$

Equation (24) can be viewed as the Tafel equation but for a 2D cell where the current density I_{cell} is corrected by the effect of the stoichiometry in the channel, i.e. $\lambda \lambda^*$. Thus, by measuring the cell overpotential and current density, it is possible to accurately fit the Tafel slope and the exchange current density to characterize the cell electrochemical kinetics.

In Figure 5, the overpotential measurement versus the corrected current density is shown for all the measurements summarised in Table 2. The methodology to compute the uncertainty of the current density is explained in appendix. The overpotential is computed as

$$\eta = 1.23 - E_{cell} - r_{HF} \times I_{cell}\ , \tag{25}$$

where E_{cell}, r_{HF} and I_{cell} are the cell voltage, ohmic resistance and current density measured. These values are summarised in Table 3, and the overpotential is plotted versus $I_{cell}\lambda\lambda^*$ in Figure 5. Using Equation (24) and a linear regression, the Tafel slope and the exchange current are obtained (see Table 3 for the values).

In their review, Eslamibidgoli et al. [3] recalled that three regimes of electrochemical kinetics are theoretically expected. From medium to high overpotentials, these regimes are characterised by a value of Tafel slope that varies from 80 mV to 120 mV [3]. Our results presented in Figure 5 show a similar trend where the slope varies between the data points measured at medium and high overpotential with a Tafel slope equal to 143 ± 21 mV and 229 ± 52 mV, respectively. We found that the value of the Tafel slope is larger than what is theoretically predicted, but the ratio between them is correct (2/3). The larger than expected Tafel slopes measured in his study are in-situ values in sense that some other physical phenomena may have impacted it: heterogeneities in the fuel cell assembly, effect of the channel/rib, catalyst degradations/aging. However, this Tafel slope can be considered as the correct values in the framework of the stoichiometric regime and become an accurate criterion to assess the kinetic performances of different fuel cell assemblies for example.

A similar conclusion can be drawn concerning the value of the exchange currents. We found two regimes at medium and high overpotential where the values of i_c vary significatively. Although it is difficult to link these in situ values to fuel cell characteristics (platinum loading, ECSA, catalyst layer composition…), they can be used in the similar way as the Tafel slope: using i_c to characterize the fuel cell kinetics in the framework of the stoichiometric regime and compare them to study different catalyst layer or aging impact for example.

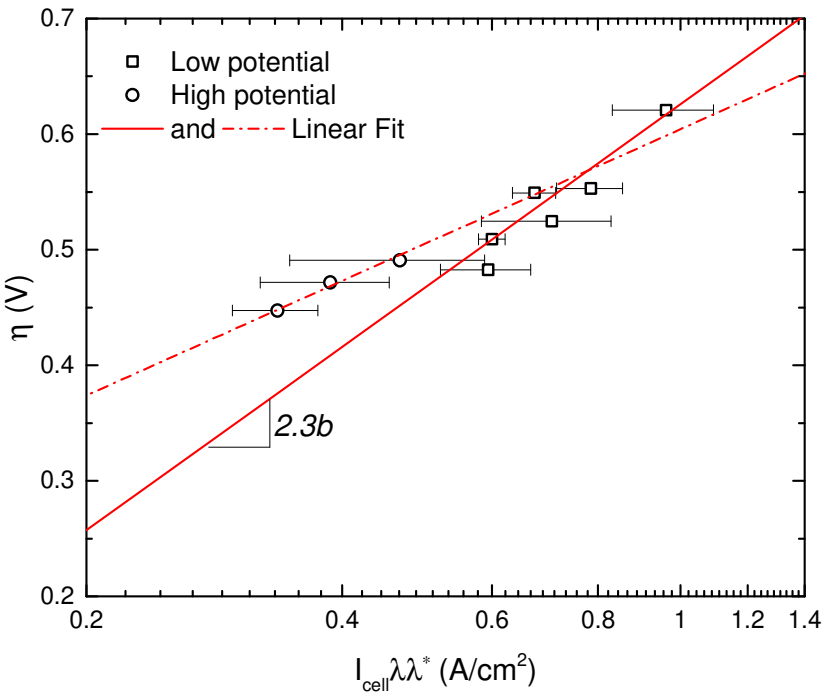

Figure 5. Linear fit of the Tafel slope and exchange current density in the stoichiometric regime.

Current (A)	I_{cell} (A/cm^2)	λ	r_{HF} (mΩ)	E (V)	η (V)	b (mV)	i_c (mA/cm^2)	α_c
6	0.500	1.29	13	0.53	0.62	229 ± 52	65 ± 18	1,01
3	0.250	1.32	16	0.69	0.49	143 ± 21	21 ± 4	0,96
4.5	0.375	1.31	15	0.64	0.52	229 ± 52	65 ± 18	0,89
6	0.500	1.60	13	0.60	0.55	229 ± 52	65 ± 18	0,91
3	0.250	1.63	16	0.71	0.47	143 ± 21	21 ± 4	1,01
4.5	0.375	1.58	15	0.68	0.48	229 ± 52	65 ± 18	0,89
6	0.500	2.14	13	0.60	0.55	229 ± 52	65 ± 18	1,06

3	0.250	2.16	14	0.74	0.45	143 ± 21	21 ± 4	1,01
6	0.500	3.18	13	0.65	0.51	229 ± 52	65 ± 18	1,00

Table 3. Summary of the fuel cell characterisation in stoichiometric regime for a range of current and oxygen stoichiometry.

3.2.2 Model validation

Going further to validate the consistency of the measured value of b and i_c with the stoichiometric regime, we check the assumption made in section 2 where $\alpha_c = i_c/j_0 e^{\eta(t)/b} \approx 1$. In the stoichiometric regime, we can write that $\alpha_c = i_c e^{\frac{\eta(t)}{b}}/(I_{cell}\lambda\lambda^*)$. These values are computed in Table 3. As it can be observed, α_c is found to be very close to 1 validating the assumption made earlier and meaning that the value b and i_c are consistent with the assumptions made to derive the stoichiometric model.

The second validation is based on the fuel cell impedance modulus. Only the phase was used previously to verify that the fuel cell is operating in stoichiometric regime. To compute the dimensionless measured fuel cell impedance, $|Z_{exp}|$, the charge transfer resistance is needed as it is shown in Equation (16). The charge transfer resistance is given by $R_{ct} = b/(j_0)$ with $j_0 = I_{cell}\lambda\lambda^*$ according to Equation (23). The uncertainty associated to the dimensionless modulus is given in appendix. These data are presented in Figure 6 and compared to the modulus of the impedance in stoichiometric regime given by Equation (14) as $|\tilde{Z}| = |1/\tilde{Z}|^{-1}$.

The experimental modulus measured in stoichiometric regime scales quite well with the model (red lines in Figure 6) for all the oxygen stoichiometries. Although some deviations can be observed (at λ = 2.15 and 3 A for example), the general trend is well reproduced. This result

shows that the fuel cell can be fully characterized where all the parameters of the stoichiometric regime can be measured (membrane resistance, electrochemical kinetics, oxygen transport in the channel) and use to predict both the steady state of the cell (current and current density) and periodic state (fuel cell impedance).

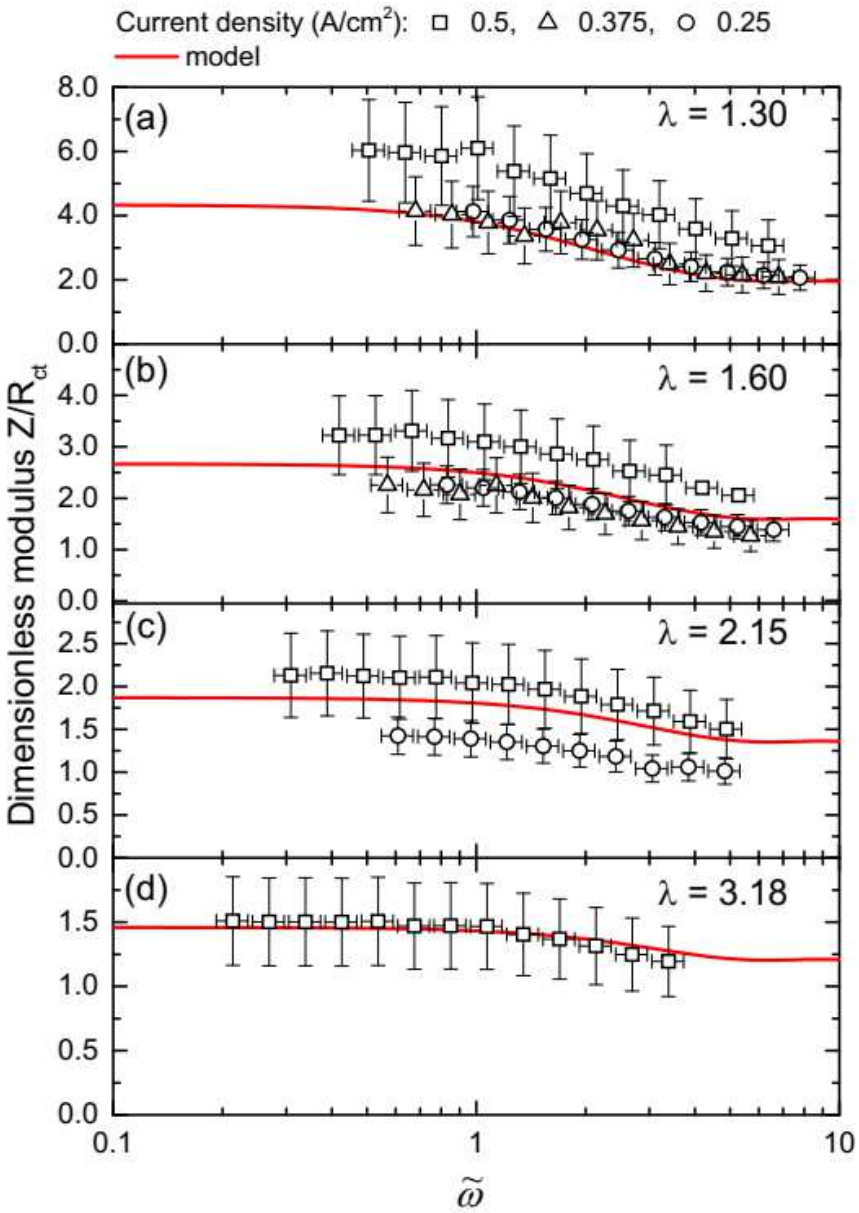

Figure 6. Impedance modulus versus dimensionless frequency for a range of air stoichiometry and cell current.

4. Conclusions

The aim of this paper was to evidence the stoichiometric regime in an operating fuel cell both at the global and local scale using EIS measurements and current density distribution measurements with a segmented flow field. This was successfully done for a range of stoichiometry from 1.30 to 3.18 and a range of current from 3 A to 6 A (0.25 to 0.5 A/cm^2). At the local scale it may have been easier to evidence the stoichiometric regime, particularly at λ = 3.18 where the low frequency phase can be altered by the oxygen transport in the GDL (see ref [16]). However, the use of segmented cell is not mandatory to obtain a signature of the stoichiometric regime since it is well observed through the low frequency phase for most of the measurements presented in this paper.

Operating a fuel cell in this particular regime is a great advantage from the modelling point of view as only two equations govern the main physical mechanisms. Therefore, few parameters are needed to predict the fuel cell behavior. Moreover, in the case they are not known, such as the kinetics parameters (Tafel slope and exchange current), a methodology is presented to measure them accurately. Thus, within the framework of this stoichiometric regime, PEM fuel cells can be better controlled, their performances better predicted, and their physical properties better characterized.

Another application of these works concerns the hydrogen/oxygen fuel cells where mass transport in the GDL are not limiting. Thus, these fuel cells operating conditions fall within the assumption needed to derive the stoichiometric regime, and our work can be transpose to this

technology to characterise the kinetic parameters or to control hydrogen/oxygen fuel cell performances.

5. Appendix – Uncertainty calculations

Dimensionless current

We consider that the N current densities measured by the segmented current collector are known within ±10% of the measured value. So, the uncertainty on the mean value is:

$$u_{mean} = \frac{0.1}{N}\sqrt{\sum_{n=1}^{N} j_n^2}, \tag{A.1}$$

This is the root sum of squares of the measured current density.

Thus, one can deduce that the uncertainty of the dimensionless current is:

$$u_{I_{adim}} = 0.1 I_{adim}\sqrt{1 + \frac{\sum_{n=1}^{N} j_n^2}{N^2 I_{mean}^2}}, \tag{A.2}$$

Flow rate, velocity and stoichiometry

In this study, the air flow rate, velocity and stoichiometry are considered to be known at ±10%. This uncertainty stems from the mass flow controller, the cell temperature controller and the back pressure controller. For sake of simplicity, all these uncertainties are embedded in a single one where the velocity is assumed to known at ±10% of u_c.

Tafel slope

Calculation of the uncertainty on the Tafel slope and the exchange current density obtained from the linear fit. For the Tafel slope, it is trivial: $u_b = u_{a_1}/2.3$ where u_{a_1} is the uncertainty computed by the linear fit including the weight of each data (error bar on x-axis). Concerning the

exchange current, it is given by the following formula: $i_c = 10^{-a_2/a_1}$ where a_1 and a_2 are the slope and the intercept, respectively. Thus, the uncertainty on i_c is given by:

$$u_{i_c}^2 = \left(u_{a_1}\frac{\partial i_c}{\partial a_1}\right)^2 + \left(u_{a_2}\frac{\partial i_c}{\partial a_2}\right)^2, \tag{A.3}$$

which lead to

$$u_{i_c} = i_c\sqrt{\frac{u_{a_2}^2}{a_2^2} + \frac{u_{a_1}^2}{a_1^2}\frac{a_2^2}{a_1^2}}. \tag{A.4}$$

Modulus

The uncertainty of the modulus depends of the uncertainty of the charge transfer resistance computed as:

$$u_{R_{ct}}^2 = \left(\frac{u_b}{\lambda\lambda^* I_{cell}}\right)^2 + u_\lambda^2\frac{b^2}{I_{cell}^2}\left(\frac{(1-\lambda)\lambda^* + 1}{(1-\lambda){\lambda^*}^2\lambda^2}\right)^2, \tag{A.5}$$

which lead to

$$\frac{u_{R_{ct}}^2}{R_{ct}^2} = \left(\frac{u_b}{b}\right)^2 + \frac{u_\lambda^2}{\lambda^2}\left(\frac{(1-\lambda)\lambda^* + 1}{(1-\lambda)\lambda^*}\right)^2. \tag{A.6}$$

Where $u_\lambda = 0.1 \times \lambda$ and u_b is given in Table 3. Finally, one can obtain

$$u_{R_{ct}} = R_{ct}\sqrt{\left(\frac{u_b}{b}\right)^2 + 0.1^2\left(\frac{(1-\lambda)\lambda^* + 1}{(1-\lambda)\lambda^*}\right)^2}, \tag{A.7}$$

and, the uncertainty on the dimensionless modulus is given by

$$u_{|\tilde{Z}|} = |\tilde{Z}| \frac{u_{Rct}}{R_{ct}}. \tag{A.8}$$

Acknowledgements

The research leading to these results received funding from the People Programme (Marie Curie Actions) of the European Union's Seventh Framework Programme (FP7/2007-2013) under REA grant agreement n° PCOFUND-GA-2013-609102, through the PRESTIGE programme coordinated by Campus France. The authors would like to gratefully acknowledge Mr Christophe Le Bozec for his help in designing and building the experimental setup.

References

[1] N. Konno, S. Mizuno, H. Nakaji, Y. Ishikawa, *Development of Compact and High-Performance Fuel Cell Stack*, SAE Int. J. Altern. Powertrains. **4** (2015) 2015-01–1175.

[2] T. Yoshida, K. Kojima, *Toyota MIRAI Fuel Cell Vehicle and Progress Toward a Future Hydrogen Society*, Interface Mag. **24** (2015) 45–49.

[3] M.J. Eslamibidgoli, J. Huang, T. Kadyk, A. Malek, M. Eikerling, *How theory and simulation can drive fuel cell electrocatalysis*, Nano Energy. **29** (2016) 334–361.

[4] A.Z. Weber, R.L. Borup, R.M. Darling, P.K. Das, T.J. Dursch, W. Gu, et al., *A Critical Review of Modeling Transport Phenomena in Polymer-Electrolyte Fuel Cells*, J. Electrochem. Soc. **161** (2014) F1254–F1299.

[5] A.Z. Weber, J. Newman, *Modeling Transport in Polymer-Electrolyte Fuel Cells*, Chem. Rev. **104** (2004) 4679–4726.

[6] A.A. Kulikovsky, *The effect of stoichiometric ratio λ on the performance of a polymer electrolyte fuel cell*, Electrochim. Acta. **49** (2004) 617–625.

[7] J.T. Gostick, *Versatile and efficient pore network extraction method using marker-based watershed segmentation*, Phys. Rev. E. **96** (2017) 023307.

[8] L. Cindrella, A.M. Kannan, J.F. Lin, K. Saminathan, Y. Ho, C.W. Lin, J. Wertz, *Gas diffusion layer for proton exchange membrane fuel cells—A review*, J. Power Sources. **194** (2009) 146–160.

[9] G. Zhang, K. Jiao, *Multi-phase models for water and thermal management of proton exchange membrane fuel cell: A review*, J. Power Sources. **391** (2018) 120–133.

[10] B.P. Setzler, T.F. Fuller, *A Physics-Based Impedance Model of Proton Exchange Membrane Fuel Cells Exhibiting Low-Frequency Inductive Loops*, J. Electrochem. Soc. **162** (2015) F519–F530.

[11] Y. Wang, S. Basu, C.-Y. Wang, *Modeling two-phase flow in PEM fuel cell channels*, J. Power Sources. **179** (2008) 603–617.

[12] T.E. Springer, T.A. Zawodzinski, S. Gottesfeld, *Polymer Electrolyte Fuel Cell Model*, J. Electrochem. Soc. **138** (1991) 2334.

[13] A.A. Kulikovsky, *A simple equation for in situ measurement of the catalyst layer oxygen diffusivity in PEM fuel cell*, J. Electroanal. Chem. **720–721** (2014) 47–51.

[14] A.A. Kulikovsky, *The regimes of catalyst layer operation in a fuel cell*, Electrochim. Acta. **55** (2010) 6391–6401.

[15] S. Chevalier, C. Josset, B. Auvity, *Analytical solutions and dimensional analysis of pseudo 2D current density distribution model in PEM fuel cells*, Renew. Energy. **125** (2018) 738–746.

[16] S. Chevalier, C. Josset, B. Auvity, *Analytical solution for the low frequency polymer electrolyte membrane fuel cell impedance*, J. Power Sources. **407** (2018) 123–131.

[17] J. Xuan, H. Wang, D.Y.C. Leung, M.K.H. Leung, H. Xu, L. Zhang, Y. Shen, *Theoretical Graetz–Damköhler modeling of an air-breathing microfluidic fuel cell*, J. Power Sources. **231** (2013) 1–5.

[18] G. Maranzana, J. Mainka, O. Lottin, J. Dillet, A. Lamibrac, A. Thomas, S. Didierjean, *A proton exchange membrane fuel cell impedance model taking into account convection along the air channel: On the bias between the low frequency limit of the impedance and the slope of the polarization curve*, Electrochim. Acta. **83** (2012) 13–27.

[19] K.T. Jeng, C.P. Kuo, S.F. Lee, *Modeling the catalyst layer of a PEM fuel cell cathode using a dimensionless approach*, J. Power Sources. **128** (2004) 145–151.

[20] O. Shamardina, M.S. Kondratenko, A.V. Chertovich, A. Kulikovsky, *A simple transient model for a high temperature PEM fuel cell impedance*, Int. J. Hydrogen Energy. **39** (2014) 2224–2235.

[21] J.-C. Olivier, G. Wasselynck, S. Chevalier, B. Auvity, C. Josset, D. Trichet, G. Squadrito, N. Bernard, *Multiphysics modeling and optimization of the driving strategy of a light duty fuel cell vehicle*, Int. J. Hydrogen Energy. **42** (2017) 26943–26955.

[22] N. Fouquet, C. Doulet, C. Nouillant, G. Dauphin-Tanguy, B. Ould-Bouamama, *Model based PEM fuel cell state-of-health monitoring via ac impedance measurements*, J. Power Sources. **159** (2006) 905–913.

[23] I. Manke, C. Hartnig, M. Grünerbel, W. Lehnert, N. Kardjilov, A. Haibel, A. Hilger, J. Banhart, H. Riesemeier, *Investigation of water evolution and transport in fuel cells with high resolution synchrotron x-ray radiography*, Appl. Phys. Lett. **90** (2007) 174105.

[24] J. Lee, S. Chevalier, R. Banerjee, P. Antonacci, N. Ge, R. Yip, T. Kotaka, Y. Tabuchi, A. Bazylak, *Investigating the effects of gas diffusion layer substrate thickness on polymer electrolyte membrane fuel cell performance via synchrotron X-ray radiography*, Electrochim. Acta. **236** (2017) 161–170.

[25] D. Hayashi, A. Ida, S. Magome, T. Suzuki, S. Yamaguchi, R. Hori, *Synchrotron X-Ray Visualization and Simulation for Operating Fuel Cell Diffusion Layers*, in: 2017.

[26] Q. Meyer, Y. Zeng, C. Zhao, *In Situ and Operando Characterization of Proton Exchange Membrane Fuel Cells*, Adv. Mater. (2019) 1901900.

[27] G. Hinds, *In situ diagnostics for polymer electrolyte membrane fuel cells*, Curr. Opin. Electrochem. **5** (2017) 11–19.

[28] J.E.B. Randles, *Kinetics of Rapid Electrode Reactions*, Discuss. Faraday Soc. **1** (1947) 11–19.

[29] P. Antonacci, S. Chevalier, J. Lee, N. Ge, J. Hinebaugh, R. Yip, Y. Tabuchi, T. Kotaka, A. Bazylak, *Balancing mass transport resistance and membrane resistance when tailoring*

MPL thickness for PEM fuel cells, Electrochim. Acta. **188** (2016) 888–897.

[30] T.E. Springer, T.A. Zawodzinski, M.S. Wilson, S. Golfesfeld, *Characterization of Polymer Electrolyte Fuel Cells Using AC Impedance Spectroscopy*, J. Electrochem. Soc. **143** (1996) 587–599.

[31] D. Kramer, I.A. Schneider, A. Wokaun, G.G. Scherer, *Oscillations in the Gas Channels - The Forgotten Player in Impedance Spectroscopy in Polymer Electrolyte Fuel Cells B. Modeling the Wave*, in: ECS Trans., ECS, 2006: pp. 1249–1258.

[32] S.M. Rezaei Niya, M. Hoorfar, *Study of proton exchange membrane fuel cells using electrochemical impedance spectroscopy technique – A review*, J. Power Sources. **240** (2013) 281–293.

[33] L.C. Pérez, L. Brandão, J.M. Sousa, A. Mendes, *Segmented polymer electrolyte membrane fuel cells—A review*, Renew. Sustain. Energy Rev. **15** (2011) 169–185.

[34] I.A. Schneider, D. Kramer, A. Wokaun, G.G. Scherer, *Oscillations in gas channels: II. Unraveling the characteristics of the low frequency loop in air-fed PEFC impedance spectra*, J. Electrochem. Soc. **154** (2007) B770–B782.

[35] Q. Meyer, K. Ronaszegi, J.B. Robinson, M. Noorkami, O. Curnick, S. Ashton, A. Danelyan, T. Reisch, P. Adcock, R. Kraume, P.R. Shearing, D.J.L. Brett, *Combined current and temperature mapping in an air-cooled, open-cathode polymer electrolyte fuel cell under steady-state and dynamic conditions*, J. Power Sources. **297** (2015) 315–322.

[36] T. Reshetenko, A. Kulikovsky, *Comparison of Two Physical Models for Fitting PEM Fuel Cell Impedance Spectra Measured at a Low Air Flow Stoichiometry*, J. Electrochem. Soc. **163** (2016) F238–F246.

[37] N. Zamel, A. Bhattarai, D. Gerteisen, *Measurement of Spatially Resolved Impedance Spectroscopy with Local Perturbation*, Fuel Cells. **13** (2013) 910–916.

[38] G. Maranzana, O. Lottin, T. Colinart, S. Chupin, S. Didierjean, *A multi-instrumented polymer exchange membrane fuel cell: Observation of the in-plane non-homogeneities*, J. Power Sources. **180** (2008) 748–754.

[39] A. Kulikovsky, *Analytical Impedance of Oxygen Transport in a PEM Fuel Cell Channel*, J. Electrochem. Soc. **166** (2019) F306–F311.

[40] I.A. Schneider, S.A. Freunberger, D. Kramer, A. Wokaun, G.G. Scherer, *Oscillations in Gas Channels. Part I. The Forgotten Player in Impedance Spectroscopy in PEFCs*, J. Electrochem. Soc. **154** (2007) B383–B388.

[41] I. Pivac, F. Barbir, *Inductive phenomena at low frequencies in impedance spectra of proton exchange membrane fuel cells – A review*, J. Power Sources. **326** (2016) 112–119.

[42] I.J. Halvorsen, I. Pivac, D. Bezmalinović, F. Barbir, F. Zenith, *Electrochemical low-frequency impedance spectroscopy algorithm for diagnostics of PEM fuel cell degradation*, Int. J. Hydrogen Energy. (2019).

[43] S. Chevalier, N. Ge, J. Lee, M.G. George, H. Liu, P. Shrestha, D. Muirhead, N. Lavielle, B.D. Hatton, A. Bazylak, *Novel electrospun gas diffusion layers for polymer electrolyte membrane fuel cells: Part II. In operando synchrotron imaging for microscale liquid water transport characterization*, J. Power Sources. **352** (2017) 281–290.

[44] T. Reshetenko, A. Kulikovsky, *On the distribution of local current density along a PEM fuel cell cathode channel*, Electrochem. Commun. **101** (2019) 35–38.

[45] A.A. Kulikovsky, *Semi-analytical 1D+1D model of a polymer electrolyte fuel cell*, Electrochem. Commun. **6** (2004) 969–977.

[46] N. Kulkarni, Q. Meyer, J. Hack, R. Jervis, F. Iacoviello, K. Ronaszegi, P. Adcock, P.R. Shearing, D.J.L. Brett, *Examining the effect of the secondary flow-field on polymer electrolyte fuel cells using X-ray computed radiography and computational modelling*, Int. J. Hydrogen Energy. **44** (2019) 1139–1150.